XAFS Study of Tungsten L_1-, L_3-Edges: Structural Analysis of Loaded Tungsten Oxide Species

A realization of low-temperature NO*x* reduction from an exhaust gas at stationary emission sources, such as factories, boilers, power stations and incinerators, is strongly desired. In addition, some ammonia slips from factories and pig and poultry farms are serious problems from an environmental viewpoint. We found that a TiO_2-based photocatalyst is effective for the abatement of NO (photo-SCR) and the removal of NH_3 (photo-SCO), and that the loading of tungsten (W) oxide species on TiO_2 promotes photocatalyses [1,2]. Not only the loading amount but also the local structure of W oxide species affects the activities. A conventional XAFS analytical method could give us only a vague result for the structure of the loaded W oxide species.

W L_1- and L_3-edge X-ray absorptions have often been used to provide information on the local symmetry, coordination and valence of W oxide species loaded on supports [3]. The valence of the W oxide species is determined by the position of the W L_1-edge. The local symmetry is determined by the area of the pre-edge peak in W L_1-edge XANES. The coordination number and bond distance of the W oxide species are estimated by the analysis of W L_3-edge EXAFS. However, the study of W L_3-edge XANES is limited.

The white line appearing in the L_3-edge XANES of transition metals is mainly attributed to electronic transitions from $2p_{3/2}$ orbitals to vacant *d* orbitals. In the case of Mo L_3-edge X-ray absorption, two white lines are observed in the XANES. The splitting and areas of the two white lines depend on the symmetry of the MoO*x* ($x = 4$, 5, 6) unit because these correspond to the ligand field splitting of the *d* orbitals [4]. Therefore, it is expected that W L_3-edge XANES will reveal the characteristics of the 5*d* orbitals in a manner similar to that of Mo L_3-edge XANES. However, no such relationship between W L_3-edge XANES and the structure has been described. This is because the white line is not distinctly split as is the case for Mo [5].

In the present study, we recorded the W L_1- and L_3-edge X-ray absorption spectra of reference samples, whose structures are already known, at beamline **BL01B1** in a transmission mode. We analyzed the W L_3-edge XANES carefully to clarify the relationship between the splitting of the W L_3-edge white line and the structure of the WO*x* unit. Additionally, we found that the structure of the WO*x* unit can be estimated from the splitting of the W L_3-edge white line and the pre-edge peak area of the W L_1-edge XANES. This new structural analysis method can also easily estimate the structure of the W^{6+} oxide loaded on TiO_2.

Figure 1(A) shows the W L_3-edge XANES spectra of reference samples with the W^{6+} ion. Cr_2WO_6 and Ba_2NiWO_6, which have D_2 and *Oh* symmetries, give two peaks in the white line. On the other hand, WO_3, $H_3PW_{12}O_{40}$, and $(NH_4)_{10}W_{12}O_{41}{\cdot}5H_2O$ samples, which have a distorted WO_6 unit, and $Sc_2W_3O_{12}$ and Na_2WO_4, which respectively have nearly *Td* and *Td* symmetries, exhibit only one peak. However, the second derivatives of the W L_3-edge white line clarify that the white line consists of two peaks ($Sc_2W_3O_{12}$ and Na_2WO_4 give a large peak with a shoulder peak at a low energy), as shown in Fig. 1(B). In general, 5*d* orbitals of the octahedral (tetrahedral) WO_6 (WO_4) unit are split into e_g and t_{2g} (*e* and t_g) orbitals by a ligand field. The poorer the symmetry of WO_6 (WO_4) from *Oh* (*Td*), the smaller (larger) the energy gap of the split 5*d* orbitals. Additionally, the energy gap for the WO_4 unit is smaller than that for the WO_6 unit. Therefore, the energy gap of the two peaks in Fig. 1(B) reflects the splitting of 5*d* orbitals by the ligand field. Additionally, we carried out the deconvolution of the W L_3-edge XANES spectra. All spectra were fitted with two Lorentz functions, whose top positions were determined on the basis of the values of the two peaks in Fig. 1(B), and an arctangent function. Figure 2 shows the results of the deconvolution of WO_3 and Na_2WO_4, as examples. The ratio of the areas under the two peaks (peak 1: peak 2; peak 1 appears at a lower energy than peak 2) for the samples with the WO_6 unit was about 3:2, whereas that for the sample with the WO_4 unit was about 2:3. For the WO_6 (WO_4) unit, the t_{2g} (*e*) orbital appears at a

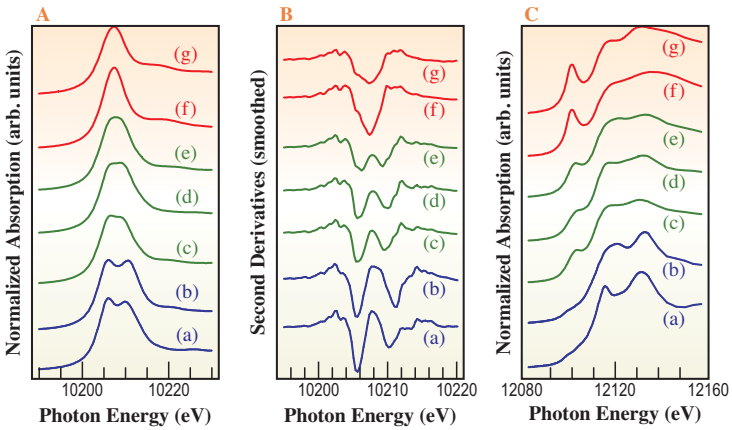

Fig. 1. **(A)** W L_3-edge XANES spectra, **(B)** second derivatives of **(A)**, and **(C)** W L_1-edge XANES spectra of (a) Ba_2NiWO_6, (b) Cr_2WO_6, (c) $(NH_4)_{10}W_{12}O_{41}{\cdot}5H_2O$, (d) WO_3, (e) $H_3PW_{12}O_{40}{\cdot}13H_2O$, (f) $Sc_2W_3O_{12}$ and (g) Na_2WO_4.

lower energy than the e_g (t_g) orbital and the X-ray absorption intensity is t_{2g}:e_g=3:2 (e:t_g=2:3). Thus, the ratios of peak 1:peak 2 reflect the absorption intensities of the split 5*d* states. From the above results, we conclude that the white line in the W L_3-edge XANES indicates the electron transition from the $2p_{3/2}$ orbital to the split 5*d* orbitals.

Figure 1(C) shows the W L_1-edge XANES spectra of the reference samples. The pre-edge peak is mainly attributed to the forbidden electron transition from a 2*s* orbital to 5*d* orbitals. The less symmetric structure of W oxide species (distortion from the *Oh* symmetry) provides a larger pre-edge peak because this forbidden electron transition is induced by mixing p orbitals of tungsten and ligand into empty d orbitals. Therefore, Na_2WO_4 and $Sc_2W_3O_{12}$ exhibit a large pre-edge peak. We found that the combination of the area of the pre-edge peak of the W L_1-edge XANES and the splitting of the W L_3-edge white line provides more reliable information on the structure of the W oxide species. Figure 3 shows the area of the pre-edge peak of the W L_1-edge XANES plotted against the energy gap of the split W L_3-edge white line for the reference samples (represented by red solid circle). Figure 3 reveals an interesting relationship, in that the area of the pre-edge peak has a linear correlation with the energy gap of the split W L_3-edge white line. This linear relationship is supported by density functional theory calculations of the octahedral and tetrahedral W models [2]. Therefore, we conclude that the structure of the W oxide species can be easily estimated by a combination of the pre-edge peak area of the W L_1-edge XANES and the energy gap of the split W L_3-edge white line.

Using this new analytical method, we estimated the structure of the W oxide species loaded on TiO_2 samples from the above linear correlation. The samples used were *x*(2, 4, 12, 20, 40, and 80) molg^{-1} $H_3PW_{12}O_{40}\cdot 13H_2O$ loaded on TiO_2 (*x*HPA/TiO_2). The area of the pre-edge peak of W L_1-edge XANES is plotted against the energy gap of the split W L_3-edge white line for *x*HPA/TiO_2 in Fig. 3 (represented by blue solid square). As shown in Fig. 3, 2HPA/TiO_2 has a WO_6 structure and the amount of WO_4 species increases with an increase in the amount of loaded HPA. These estimated structures of W oxide species were in agreement with the curve fitting analysis results for the W L_3-edge EXAFS [2].

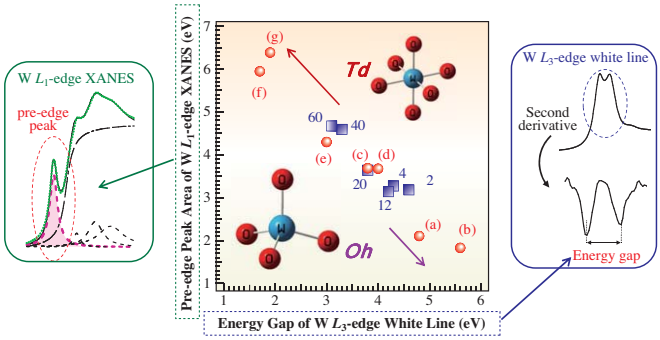

Fig. 3. Dependence of pre-edge peak area of W L_1-edge XANES on energy gap of split W L_3-edge white line of reference samples; (red solid circle): reference samples ((**a**) Ba_2NiWO_6, (**b**) Cr_2WO_6, (**c**) $(NH_4)_{10}W_{12}O_{41}\cdot 5H_2O$, (**d**) WO_3, (**e**) $H_3PW_{12}O_{40}\cdot 13H_2O$, (**f**) $Sc_2W_3O_{12}$ and (**g**) Na_2WO_4), (blue solid square): *x*HPA/TiO_2 samples (*x*=2, 4, 12, 20, 40, 60).

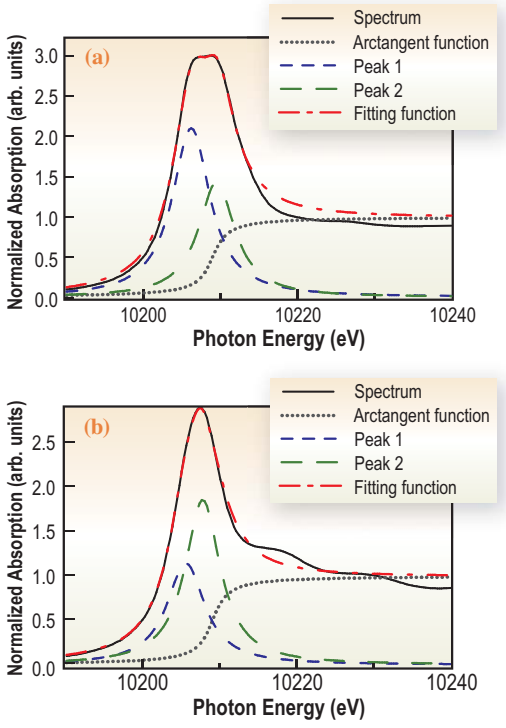

Fig. 2. Deconvolution of W L_3-edge XANES spectra of (**a**) WO_3 and (**b**) Na_2WO_4.

Seiji Yamazoe[a,*], Tetsuya Shishido[b] and Tsunehiro Tanaka[b]

[a] Dept. of Materials Chemistry, Ryukoku University
[b] Dept. of Molecular Engineering, Kyoto University

*E-mail: yamazoe@rins.ryukoku.ac.jp

References

[1] S. Yamazoe *et al.*: Appl. Catal. B **83** (2008) 123.
[2] *S. Yamazoe, Y. Hitomi, T. Shishido and T. Tanaka: J. Phys. Chem. C* ***112*** *(2008) 6869.*
[3] M. Fernández-García *et al.*: J. Phys. Chem B **109** (2005) 6075.
[4] G.N. George *et al.*: J. Am. Chem. Soc. **112** (1990) 2541.
[5] F. Hilbrig *et al.*: J. Phys. Chem. **95** (1991) 6973.